LETTER

Heat dissipation in atomic–scale junctions

Woochul Lee[1]*, Kyeongtae Kim[1]*, Wonho Jeong[1], Linda Angela Zotti[2], Fabian Pauly[3], Juan Carlos Cuevas[2] & Pramod Reddy[1,4]

Atomic and single-molecule junctions represent the ultimate limit to the miniaturization of electrical circuits[1]. They are also ideal platforms for testing quantum transport theories that are required to describe charge and energy transfer in novel functional nanometre-scale devices. Recent work has successfully probed electric and thermoelectric phenomena[2–8] in atomic-scale junctions. However, heat dissipation and transport in atomic-scale devices remain poorly characterized owing to experimental challenges. Here we use custom-fabricated scanning probes with integrated nanoscale thermocouples to investigate heat dissipation in the electrodes of single-molecule ('molecular') junctions. We find that if the junctions have transmission characteristics that are strongly energy dependent, this heat dissipation is asymmetric—that is, unequal between the electrodes—and also dependent on both the bias polarity and the identity of the majority charge carriers (electrons versus holes). In contrast, junctions consisting of only a few gold atoms ('atomic junctions') whose transmission characteristics show weak energy dependence do not exhibit appreciable asymmetry. Our results unambiguously relate the electronic transmission characteristics of atomic-scale junctions to their heat dissipation properties, establishing a framework for understanding heat dissipation in a range of mesoscopic systems where transport is elastic—that is, without exchange of energy in the contact region. We anticipate that the techniques established here will enable the study of Peltier effects at the atomic scale, a field that has been barely explored experimentally despite interesting theoretical predictions[9–11]. Furthermore, the experimental advances described here are also expected to enable the study of heat transport in atomic and molecular junctions—an important and challenging scientific and technological goal that has remained elusive[12,13].

Charge transport is always accompanied by heat dissipation (Joule heating). This process is well understood at the macroscale, where the power dissipation (heat dissipated per unit time) is volumetric and is given by $j^2\rho$, where j is the magnitude of the current density and ρ is the electrical resistivity. Heating in atomic-scale junctions is expected to be fundamentally different, as charge transport through such junctions is largely elastic[14,15]. Recent experiments have probed the local non-equilibrium electronic and phononic temperatures in molecular junctions[16–18] to obtain insights into the effect of electron–electron and electron–phonon interactions on heat dissipation at the atomic scale. However, experimental challenges in quantitatively measuring atomic-scale heat dissipation have impeded the elucidation of a fundamental question: what is the relationship between the electronic transmission characteristics of atomic and molecular junctions (AMJs) and their heat dissipation properties?

In this work, we overcome this challenging experimental hurdle by using custom-fabricated nanoscale–thermocouple integrated scanning tunnelling probes (NTISTPs; Fig. 1a and b). The NTISTPs feature an outer gold (Au) electrode that is electrically isolated but thermally well connected to the integrated gold-chromium thermocouple via a thin (70 nm) silicon nitride film (see Supplementary Information for fabrication details). To probe heat dissipation, we first created a series of AMJs (Fig. 1c) between the outer Au electrode of the NTISTP and a flat Au substrate. Application of a voltage bias across such AMJs results in a temperature rise of the integrated thermocouple due to heat dissipation in the NTISTP's apex on a length scale comparable to the inelastic mean free path of electrons in Au (ref. 19). The power dissipation in the probe (Q_P) and the temperature rise of the thermocouple (ΔT_{TC}), located ~300 nm away from the apex, are directly related by $Q_P = \Delta T_{TC}/R_P$ (see Methods), where R_P is the thermal resistance of the NTISTP (see Fig. 1b). Further, ΔT_{TC} is related to the thermoelectric voltage output of the thermocouple (ΔV_{TC}) by $\Delta V_{TC} = -S_{TC}\Delta T_{TC}$, where S_{TC} is the effective Seebeck coefficient of the thermocouple. We note that R_P and S_{TC} were experimentally determined to be $72,800 \pm 500\,\mathrm{K\,W^{-1}}$ and $16.3 \pm 0.2\,\mathrm{\mu V\,K^{-1}}$, respectively (Supplementary Information).

We began our experimental studies, at room temperature, by trapping single molecules of 1,4-benzenediisonitrile (BDNC; Fig. 1c) between the Au electrodes of the NTISTP and the substrate using a break junction technique[5,20]. We first obtained electrical conductance
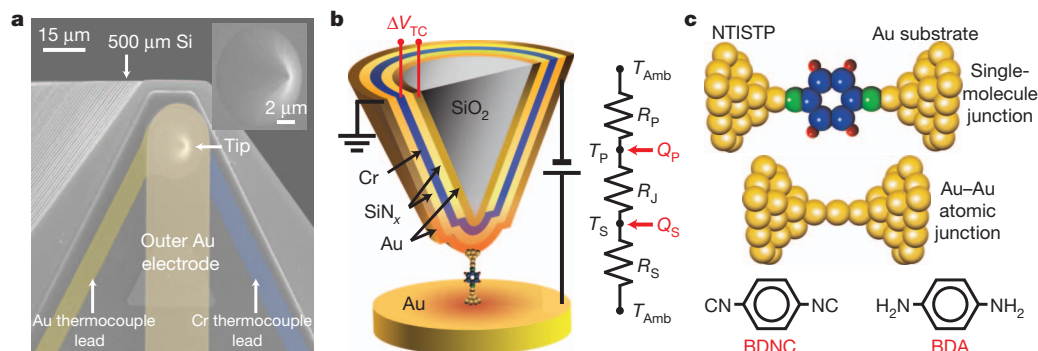
Figure 1 | Nanoscale thermocouple probes and atomic and molecular junctions studied in this work. a, Scanning electron microscope (SEM) image of a NTISTP. The electrodes are false-coloured. Inset, magnified image of the tip. **b,** Diagram of a junction created between the NTISTP (cross-sectional view) and a Au substrate (bottom) along with a thermal resistance network (right) that represents the dominant resistances to heat flow. **c,** Diagrams of molecular and atomic junctions (top) along with the structures of the molecules studied (bottom). (All diagrams are not drawn to scale or proportion.)

[1]Department of Mechanical Engineering, University of Michigan, Ann Arbor, Michigan 48109, USA. [2]Departamento de Física Teórica de la Materia Condensada and Condensed Matter Physics Center (IFIMAC), Universidad Autónoma de Madrid, Madrid 28049, Spain. [3]Department of Physics, University of Konstanz, D-78457 Konstanz, Germany. [4]Department of Materials Science and Engineering, University of Michigan, Ann Arbor, Michigan 48109, USA.
*These authors contributed equally to this work.

versus displacement traces by monitoring the electrical current under an applied bias while the NTISTP–substrate separation was systematically varied. Figure 2a shows representative conductance traces along with a histogram obtained from 500 such curves. The histogram features a peak at ~$0.002G_0$ ($G_0 = 2e^2/h \approx (12.9\,\text{k}\Omega)^{-1}$), which represents the most probable low-bias conductance of Au–BDNC–Au junctions ($G_{\text{Au-BDNC-Au}}$) and is in good agreement with past work[21].

To probe heat dissipation, we created stable Au–BDNC–Au junctions with a conductance that is within 10% of the most probable low-bias conductance[20]. We studied heat dissipation in 100 distinct Au–BDNC–Au junctions, at each bias, to obtain the time-averaged temperature rise ($\Delta T_{\text{TC,Avg}}$) and the time-averaged power dissipation in the NTISTP ($Q_{\text{P,Avg}}$) for both positive and negative biases. Here, a positive (negative) bias corresponds to a scenario where the probe is grounded, while the substrate is at a higher (lower) potential. We note that a modulated voltage bias was applied to the junctions to obtain $\Delta T_{\text{TC,Avg}}$—with high resolution—for both positive and negative biases (see Methods and Supplementary Information). This modulation scheme enables rejection of broadband noise and plays a critical role in performing high-resolution thermometry.

The circles (triangles) in Fig. 2b represent the measured $\Delta T_{\text{TC,Avg}}$ as well as the estimated $Q_{\text{P,Avg}}$ for positive (negative) biases as a function of the time-averaged total power dissipation in the junctions ($Q_{\text{Total,Avg}}$) at each bias voltage. Here, $Q_{\text{Total,Avg}}$ represents all the power dissipated in the junction, at a given bias voltage, and can be readily obtained from the measured current (I) and the known voltage bias (V) applied to the junction (see Methods). We note that the current–voltage (I–V) characteristics of Au–BDNC–Au junctions are nonlinear (Fig. 2c), therefore, in general $Q_{\text{Total,Avg}} \neq G_{\text{Au-BDNC-Au}}V^2$. The dotted line in Fig. 2b corresponds to the expected temperature rise of the probe if the heating was symmetric, that is, if half of the total power was dissipated in the probe ($\Delta T_{\text{Symmetric}} = Q_{\text{Total,Avg}}/2R_{\text{P}}$). It can be clearly seen that for a given $Q_{\text{Total,Avg}}$ the power dissipation in

the probe is larger under a negative bias than a positive bias. We also conclude that the time-averaged power dissipation in the substrate, $Q_{\text{S,Avg}}$, is smaller under a negative bias than under a positive bias, because $Q_{\text{P,Avg}} + Q_{\text{S,Avg}} = Q_{\text{Total,Avg}}$. To clarify the voltage biases used in the experiments, we present (in the inset of Fig. 2b) $\Delta T_{\text{TC,Avg}}$ as a function of the magnitude of the applied voltage bias. These results unambiguously demonstrate that heat dissipation in the electrodes of Au–BDNC–Au junctions is bias polarity dependent and unequal.

This observation raises an important question: why is the heat dissipation in the electrodes unequal in spite of the symmetric geometry of the molecular junctions? To address this question, we resort to the Landauer theory of quantum transport, which has successfully described charge transport in numerous nanostructures[19]. Within this theory, the power dissipated in the probe and the substrate, $Q_{\text{P}}(V)$ and $Q_{\text{S}}(V)$, respectively, is given by[22]:

$$Q_{\text{P}}(V) = \frac{2}{h} \int_{-\infty}^{\infty} (\mu_{\text{P}} - E)\tau(E,V)[f_{\text{P}} - f_{\text{S}}]\,dE$$

$$Q_{\text{S}}(V) = \frac{2}{h} \int_{-\infty}^{\infty} (E - \mu_{\text{S}})\tau(E,V)[f_{\text{P}} - f_{\text{S}}]\,dE \qquad (1)$$

Here μ_{P} and μ_{S} are the chemical potentials of the probe and substrate electrodes, respectively, $f_{\text{P/S}}$ represent the Fermi-Dirac distribution of the probe/substrate electrodes, and $\tau(E,V)$ is the energy (E) and voltage bias (V) dependent transmission function. Equation (1) suggests that the power dissipation in the two electrodes is, in general, unequal, that is, $Q_{\text{P}}(V) \neq Q_{\text{S}}(V)$, and bias polarity dependent, that is, $Q_{\text{P/S}}(V) \neq Q_{\text{P/S}}(-V)$. Specifically, it is straightforward to show that:

$$Q_{\text{P}}(V) - Q_{\text{P}}(-V) \approx 2GTSV + O(V^3)$$
$$Q_{\text{P}}(V) - Q_{\text{S}}(V) \approx 2GTSV + O(V^3) \qquad (2)$$
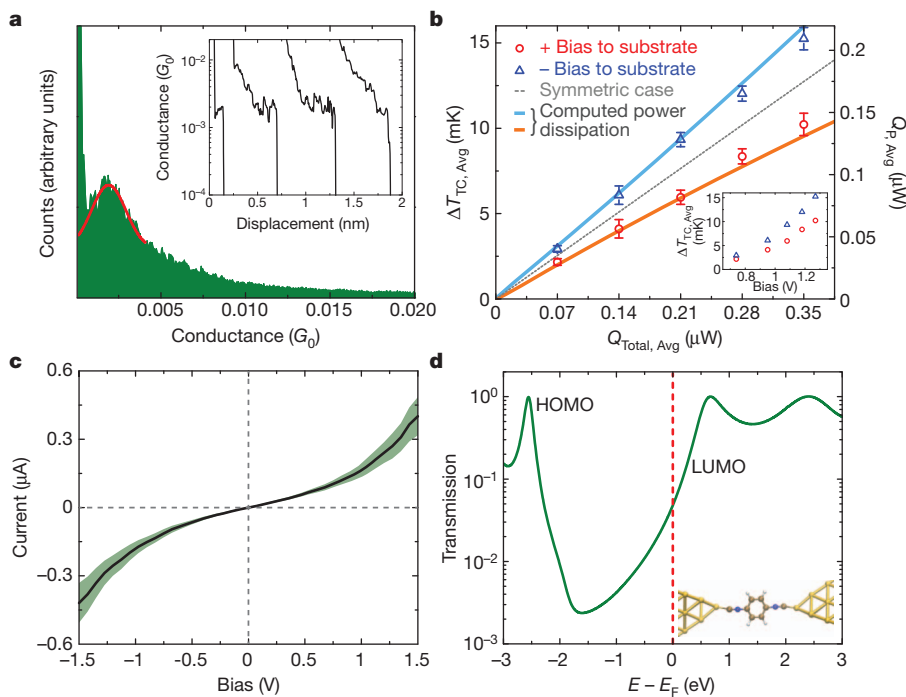
Figure 2 | Relationship between heat dissipation asymmetries and electronic transmission characteristics in Au–BDNC–Au junctions. a, Horizontally offset conductance traces (inset) of BDNC junctions, along with a histogram obtained from 500 traces (main panel). The red line represents a Gaussian fit to the histogram. **b**, Main panel, measured time-averaged temperature rise of the thermocouple ($\Delta T_{\text{TC,Avg}}$) and the time-averaged power dissipation in the probe ($Q_{\text{P,Avg}}$) as a function of the time-averaged total power dissipation in the junction ($Q_{\text{Total,Avg}}$) for positive and negative biases. Error bars represent the estimated uncertainty in $\Delta T_{\text{TC,Avg}}$ (see Supplementary Information for details of uncertainty estimation). The computationally predicted relationship between Q_{P} and Q_{Total} is shown by solid lines, which illustrates that $Q_{\text{P}} = fQ_{\text{Total}}$, where f is dependent on both Q_{Total} and the polarity of the applied bias, and is in general not equal to 0.5. The dotted line corresponds to the expected temperature rise of the probe if the heating was symmetric (that is, $f = 0.5$). Inset, measured $\Delta T_{\text{TC,Avg}}$ as a function of the magnitude of the applied voltage bias. Uncertainties are not shown in the inset, for visual clarity. **c**, I–V characteristics of Au–BDNC–Au junctions obtained by averaging 100 individual I–V curves (solid curve). The shaded region represents the standard deviation of the I–V curves. **d**, Computed zero-bias transmission function corresponding to the Au–BDNC–Au junction shown in the inset. HOMO, highest occupied molecular orbital; LUMO, lowest unoccupied molecular orbital.

Here, G is the low bias electrical conductance of the junction, T is the absolute temperature, and S is the Seebeck coefficient of the junction, whose sign is related to the first energy derivative of the zero-bias transmission $\tau'(E = E_F, V = 0)$ at the Fermi energy (E_F), resulting in a positive Seebeck coefficient for a negative first derivative and vice versa[23]. To test if the observed heating asymmetry can be understood within this framework, we computed $\tau(E, V = 0)$ for Au–BDNC–Au junctions using a transport method[24] based on density functional theory (DFT; Methods). The computed transmission function (Fig. 2d) exhibits a positive slope at the Fermi energy, in agreement with past work[25], indicating a negative Seebeck coefficient, which by virtue of equation (2) leads to higher power dissipation in the NTISTP when negative voltages are applied to the substrate. Further, the solid lines in Fig. 2b represent the relationship between Q_P and Q_{Total} ($Q_P + Q_S = Q_{Total}$) as computed from equation (1) under the assumption that $\tau(E, V)$ is well approximated by $\tau(E, V = 0)$. Notice that although our DFT approach overestimates the linear conductance, it describes correctly the relationship between Q_P and Q_{Total}. The reasons for this agreement are discussed further in the Supplementary Information, where we show in particular that this relation is relatively insensitive to the details of the junction geometry. The good agreement of the computed and measured relation between power dissipations provides strong support to the applicability of the Landauer theory of heat dissipation at the atomic scale.

To prove conclusively the relationship between electronic structure and heat dissipation, we performed additional studies on 1,4-benzenediamine (BDA; Fig. 1c) junctions, which are expected to exhibit hole-dominated electrical transport, as suggested by our calculations (Fig. 3d) and past experiments[26]. Following a procedure similar to that described above, we first determined that the most probable low-bias conductance of Au–BDA–Au junctions was $\sim 0.005G_0$ (Fig. 3a), a value consistent with past work[27]. Measurements of heat dissipation in BDA junctions (Fig. 3b) show a remarkably different asymmetry. In particular, the BDA junctions show larger power dissipation in the probe for a positive bias than for a negative one—in strong contrast to that observed in BDNC junctions. To understand this important difference, we computed the transmission function of the Au–BDA–Au junction displayed in Fig. 3d, which shows that $\tau'(E = E_F, V = 0)$ is negative,

resulting in a positive Seebeck coefficient. This, in turn, leads to larger power dissipation in the NTISTP at positive biases. Further, the computed relationship between Q_P and Q_{Total} is in good agreement with our experimental observations (solid lines in Fig. 3b).

Finally, to prove that no appreciable asymmetries are obtained if the transmission is weakly dependent on energy, we studied heat dissipation in Au–Au atomic junctions. We began our analysis by studying the conductance of Au–Au atomic junctions, which were found to have a most probable conductance of $\sim G_0$, in accordance with past studies[5,28] (Supplementary Information). Subsequently, we created 100 Au–Au atomic junctions with a low-bias conductance of $G_0 \pm 0.1G_0$ and probed heating in them. The measured $\Delta T_{TC,Avg}$ (Fig. 4a) is seen to be proportional to $Q_{Total,Avg}$ and is identical for both positive and negative biases (within experimental uncertainty, ~ 0.1 mK), clearly demonstrating that there is no detectable asymmetry in the power dissipation. Further, additional experiments performed at larger values of $Q_{Total,Avg}$ also show no detectable asymmetry (Fig. 4a inset).

Symmetric heat dissipation is indeed expected in Au–Au atomic junctions because of the weak energy dependence of their transmission function[29], which is reflected in the fact that their average thermopower vanishes[6]. In Fig. 4b we present the computed zero-bias transmission, corresponding to the Au–Au atomic junction shown in the left inset. The transmission is practically energy independent over 1 eV around the Fermi energy. This weak energy dependence results in symmetric power dissipation (from equations (1) and (2)) as well as linear I–V characteristics, as evidenced by the experimentally obtained I–V curves shown in the right inset of Fig. 4b.

The good agreement between the measured and computed asymmetries in the heat-dissipation characteristics of AMJs unambiguously confirms that heat dissipation is indeed intimately related to the transmission characteristics of the junctions, as predicted by the Landauer theory. We note that our results contradict recent claims[30] of asymmetric heat dissipation in Au atomic junctions that are not in agreement with theoretical predictions. The insights obtained here regarding heat dissipation should hold for any mesoscopic system where charge transport is predominantly elastic. Such systems include semiconductor nanowires, two-dimensional electron gases, semiconductor heterostructures, carbon nanotubes and graphene.
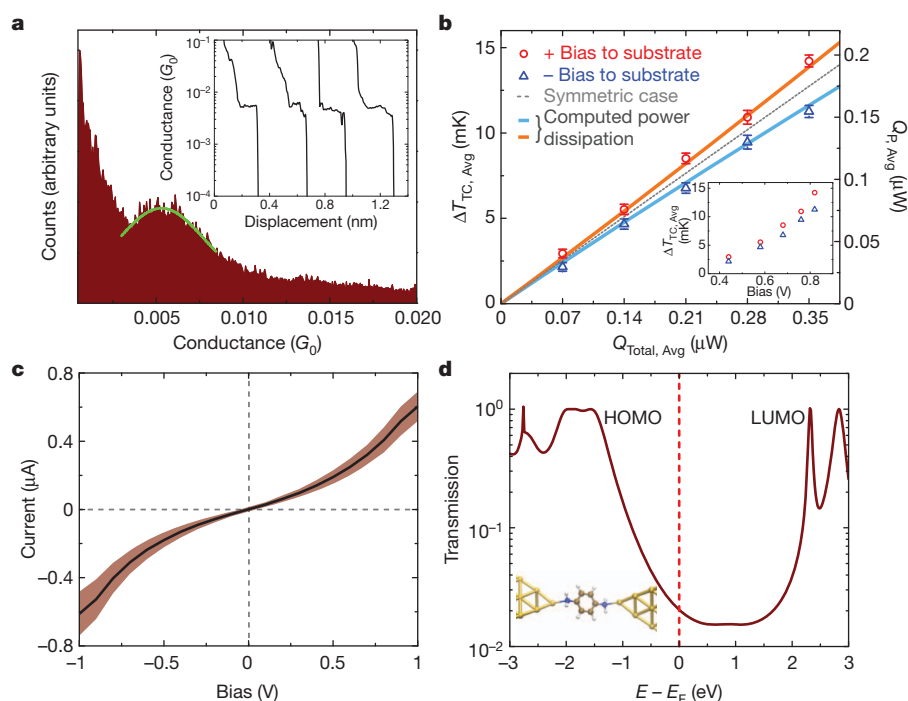
Figure 3 | Heat dissipation asymmetry for Au–BDA–Au junctions. a–d, As Fig. 2 but for Au–BDA–Au junctions. In contrast to Au–BDNC–Au junctions, the heat dissipated in the probe is found to be larger for positive biases than for negative ones.
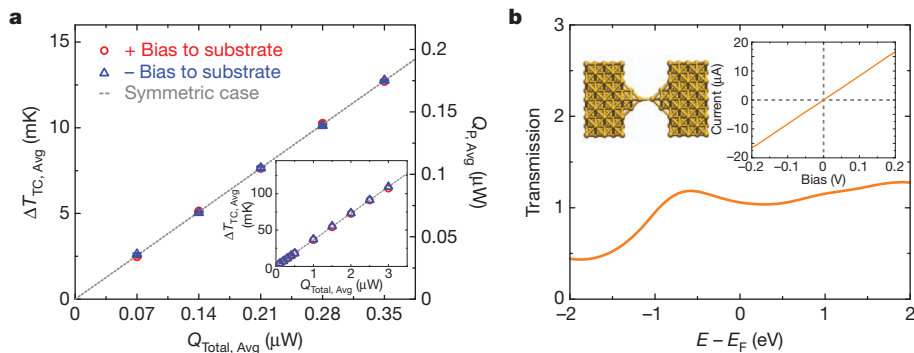
Figure 4 | No detectable heating asymmetry in Au–Au atomic junctions. a, The measured $\Delta T_{TC,Avg}$ and $Q_{P,Avg}$ in Au–Au atomic junctions for positive and negative biases as a function of $Q_{Total,Avg}$ (uncertainty of $\Delta T_{TC,Avg}$ is <0.1 mK for all voltage biases). Inset, results of similar measurements for a larger range of powers (uncertainty is <0.1 mK and is imperceptible in the figure). The measured temperature rise is found to be linearly dependent on $Q_{Total,Avg}$ and is independent of the bias polarity within experimental uncertainty. Further, $Q_{P,Avg} = Q_{Total,Avg}/2$ irrespective of the bias. **b,** The computed transmission function corresponding to the Au–Au atomic junction shown in the left inset features a weak energy dependence around the Fermi energy (E_F). Right inset shows the experimentally obtained I–V characteristics of Au–Au atomic junctions created by averaging over 100 independent I–V curves.

METHODS SUMMARY

Single-molecule and atomic junctions were created by displacing the NTISTP towards a Au substrate at $5\,nm\,s^{-1}$ and withdrawing from the substrate at $0.1\,nm\,s^{-1}$ after contact formation (indicated by an electrical conductance greater than $5G_0$). The Au substrate was coated with the desired molecules for molecular experiments and was pristine for the atomic junction studies. To obtain the conductance traces, a voltage bias of 100 mV was applied and the current was monitored during the withdrawal process. The obtained traces were analysed by creating histograms to identify the most probable conductance of AMJs. Stable single-molecule junctions with a desired conductance were created by stopping the withdrawal when a conductance plateau with a conductance within 10% of the most probable conductance was obtained. All the experiments were performed in an ultrahigh-vacuum scanning probe microscope at ambient temperature. Further, high-resolution temperature measurements were enabled by a modulation scheme where a time-dependent voltage, $V_M(t)$, consisting of a periodic series of three level voltage pulses ($+V_M$, 0 V, $-V_M$; Supplementary Fig. 1) was applied to the AMJs while monitoring the thermoelectric voltage output of the NTISTP. The zero-bias transmission functions (Figs 2–4) were computed with the *ab initio* method described in ref. 24.

Full Methods and any associated references are available in the online version of the paper.

1. Cuevas, J. C. & Scheer, E. *Molecular Electronics: An Introduction to Theory and Experiment* (World Scientific, 2010).
2. Scheer, E. *et al.* The signature of chemical valence in the electrical conduction through a single-atom contact. *Nature* **394**, 154–157 (1998).
3. Song, H. *et al.* Observation of molecular orbital gating. *Nature* **462**, 1039–1043 (2009).
4. Venkataraman, L., Klare, J. E., Nuckolls, C., Hybertsen, M. S. & Steigerwald, M. L. Dependence of single-molecule junction conductance on molecular conformation. *Nature* **442**, 904–907 (2006).
5. Xu, B. Q. & Tao, N. J. Measurement of single-molecule resistance by repeated formation of molecular junctions. *Science* **301**, 1221–1223 (2003).
6. Ludoph, B. & van Ruitenbeek, J. M. Thermopower of atomic-size metallic contacts. *Phys. Rev. B* **59**, 12290–12293 (1999).
7. Reddy, P., Jang, S. Y., Segalman, R. A. & Majumdar, A. Thermoelectricity in molecular junctions. *Science* **315**, 1568–1571 (2007).
8. Widawsky, J. R., Darancet, P., Neaton, J. B. & Venkataraman, L. Simultaneous determination of conductance and thermopower of single molecule junctions. *Nano Lett.* **12**, 354–358 (2012).
9. Galperin, M., Saito, K., Balatsky, A. V. & Nitzan, A. Cooling mechanisms in molecular conduction junctions. *Phys. Rev. B* **80**, 115427 (2009).
10. Dubi, Y. & Di Ventra, M. Colloquium: Heat flow and thermoelectricity in atomic and molecular junctions. *Rev. Mod. Phys.* **83**, 131–155 (2011).
11. Karlström, O., Linke, H., Karlström, G. & Wacker, A. Increasing thermoelectric performance using coherent transport. *Phys. Rev. B* **84**, 113415 (2011).
12. Lepri, S., Livi, R. & Politi, A. Thermal conduction in classical low-dimensional lattices. *Phys. Rep.* **377**, 1–80 (2003).
13. Li, N. B. *et al.* Colloquium: Phononics: Manipulating heat flow with electronic analogs and beyond. *Rev. Mod. Phys.* **84**, 1045–1066 (2012).
14. Agraït, N., Untiedt, C., Rubio-Bollinger, G. & Vieira, S. Onset of energy dissipation in ballistic atomic wires. *Phys. Rev. Lett.* **88**, 216803 (2002).
15. Kim, Y., Pietsch, T., Erbe, A., Belzig, W. & Scheer, E. Benzenedithiol: a broad-range single-channel molecular conductor. *Nano Lett.* **11**, 3734–3738 (2011).
16. Huang, Z. F. *et al.* Local ionic and electron heating in single-molecule junctions. *Nature Nanotechnol.* **2**, 698–703 (2007).
17. Ward, D. R., Corley, D. A., Tour, J. M. & Natelson, D. Vibrational and electronic heating in nanoscale junctions. *Nature Nanotechnol.* **6**, 33–38 (2011).
18. Ioffe, Z. *et al.* Detection of heating in current-carrying molecular junctions by Raman scattering. *Nature Nanotechnol.* **3**, 727–732 (2008).
19. Datta, S. *Electronic Transport in Mesoscopic Systems* (Cambridge Univ. Press, 1995).
20. Lee, W. & Reddy, P. Creation of stable molecular junctions with a custom-designed scanning tunneling microscope. *Nanotechnology* **22**, 485703 (2011).
21. Kiguchi, M., Miura, S., Hara, K., Sawamura, M. & Murakoshi, K. Conductance of a single molecule anchored by an isocyanide substituent to gold electrodes. *Appl. Phys. Lett.* **89**, 213104 (2006).
22. Sivan, U. & Imry, Y. Multichannel Landauer formula for thermoelectric transport with application to thermopower near the mobility edge. *Phys. Rev. B* **33**, 551–558 (1986).
23. Paulsson, M. & Datta, S. Thermoelectric effect in molecular electronics. *Phys. Rev. B* **67**, 241403 (2003).
24. Pauly, F. *et al.* Cluster-based density-functional approach to quantum transport through molecular and atomic contacts. *New J. Phys.* **10**, 125019 (2008).
25. Xue, Y. Q. & Ratner, M. A. End group effect on electrical transport through individual molecules: a microscopic study. *Phys. Rev. B* **69**, 085403 (2004).
26. Malen, J. A. *et al.* Identifying the length dependence of orbital alignment and contact coupling in molecular heterojunctions. *Nano Lett.* **9**, 1164–1169 (2009).
27. Venkataraman, L. *et al.* Single-molecule circuits with well-defined molecular conductance. *Nano Lett.* **6**, 458–462 (2006).
28. Brandbyge, M. *et al.* Quantized conductance in atom-sized wires between two metals. *Phys. Rev. B* **52**, 8499–8514 (1995).
29. Nielsen, S. K. *et al.* Current-voltage curves of atomic-sized transition metal contacts: an explanation of why Au is ohmic and Pt is not. *Phys. Rev. Lett.* **89**, 066804 (2002).
30. Tsutsui, M., Kawai, T. & Taniguchi, M. Unsymmetrical hot electron heating in quasi-ballistic nanocontacts. *Sci. Rep.* **2**, 217 (2012).

Author Contributions The idea for the experiments was conceived by P.R. and J.C.C. The experiments were performed by W.L. and K.K. The custom-fabricated probes were designed, fabricated and characterized by K.K. and W.J. *Ab initio* charge transport calculations were performed by L.A.Z. and F.P. The manuscript was written by P.R. and J.C.C. with comments and inputs from all authors.

Author Information Reprints and permissions information is available at www.nature.com/reprints. The authors declare no competing financial interests. Readers are welcome to comment on the online version of the paper. Correspondence and requests for materials should be addressed to P.R. (pramodr@umich.edu) or J.C.C. (juancarlos.cuevas@uam.es).

METHODS

Creation of atomic and molecular junctions. All the AMJs were created between a NTISTP and a Au-coated substrate by displacing the NTISTP towards a Au substrate (which was coated with the desired molecules in molecular experiments and was pristine in atomic junction experiments) at $5\,\mathrm{nm\,s^{-1}}$ and withdrawing from the substrate at $0.1\,\mathrm{nm\,s^{-1}}$ after contact formation as indicated by an electrical conductance greater than $5G_0$. To create the desired monolayers, 1 mM solutions of BDNC and BDA molecules, obtained commercially from Sigma Aldrich with a purity of $\sim$99%, were created in toluene/ethanol. Subsequently, a Au-coated mica substrate (electron beam evaporation) was placed in one of the solutions to allow self-assembly of molecules on the Au surface. After exposing the substrates for 12 h in a glove box filled with nitrogen gas, they were rinsed in ethanol and dried in nitrogen gas. For the experiments involving Au–Au atomic junctions, the Au-coated substrates were cleaned in ultraviolet-radiation ozone to eliminate any organic contamination on the surface. The NTISTPs were also cleaned with ultraviolet-radiation ozone in all studies and loaded into the UHV scanning probe microscope instrument. The measurement of electrical current was performed using a current amplifier (Keithley 428), whereas thermoelectric voltage measurements were performed using a voltage amplifier (Stanford Research System 560). All the data were collected at a sampling frequency of 2 kHz using a data acquisition system (National Instruments 6281). The approach, withdraw, and hold sequences were accomplished by using a real-time controller (National Instruments PXI8110).

Measurement of $\Delta T_{\mathrm{TC,Avg}}$ using a modulation scheme. High-resolution temperature measurements are enabled by a modulation scheme in which a time-dependent voltage, $V_{\mathrm{M}}(t)$, consisting of a periodic series of three level voltage pulses $+V_{\mathrm{M}}$, 0 V, $-V_{\mathrm{M}}$ (Supplementary Fig. 1), is applied. In all the experiments performed in this work, the period (T_{P}) of the voltage pulses was chosen to be $\sim$0.08 s (1/12.25 Hz). The selected modulation frequency is found to optimize the signal-to-noise ratio and is experimentally feasible owing to the small thermal time constants ($\sim$10 µs) of the micrometre-sized NTISTPs, which enable high-fidelity tracking of temperature changes. The applied $V_{\mathrm{M}}(t)$ results in both a modulated current ($I_{\mathrm{M}}(t)$; see Supplementary Fig. 1) and a modulated temperature change of the thermocouple ($\Delta T_{\mathrm{M,TC}}(t)$) due to Joule heating. Using the equation at the bottom of Supplementary Fig. 1, the time-averaged temperature rise corresponding to a positive bias $\Delta T_{\mathrm{TC,Avg}}(+V_{\mathrm{M}})$ or a negative bias $\Delta T_{\mathrm{TC,Avg}}(-V_{\mathrm{M}})$ can be directly related to the modulated thermoelectric voltage output ($\Delta V_{\mathrm{M,TC}}(t)$) of the thermocouple. In probing heat dissipation in AMJs we applied the modulated voltage signal with an appropriately chosen amplitude V_{M} for a period of $\sim$5 s to each AMJ. The resulting thermoelectric voltage signal $\Delta V_{\mathrm{M,TC}}(t)$ was simultaneously recorded. This was repeated on $\sim$100 junctions to collect data for $\sim$500 s for each V_{M}. The obtained data were concatenated and analysed to estimate $\Delta T_{\mathrm{TC,Avg}}$ corresponding to positive and negative biases as described above. This modulation scheme enables temperature measurements with submillikelvin resolution, as described in the Supplementary Information. The time-averaged total power dissipation ($Q_{\mathrm{Total,Avg}}$), at each bias, was obtained by using the 500-s-long data corresponding to each V_{M}. Specifically, the data (measured current and known applied bias) were used to first compute the total heat dissipated at positive and negative biases. Subsequently, $Q_{\mathrm{Total,Avg}}(+V_{\mathrm{M}}/-V_{\mathrm{M}})$ was obtained by dividing the estimated total heat dissipation (corresponding to a positive or a negative bias) by the total time during which a positive bias ($+V_{\mathrm{M}}$) or negative bias ($-V_{\mathrm{M}}$) was applied ($\sim$500/3 s). The amplitudes (V_{M}) of the three level voltage pulses used in our studies were chosen to be 30 mV, 43 mV, 52 mV, 60 mV and 67 mV for Au–Au junctions; 0.74 V, 0.95 V, 1.08 V, 1.18 V and 1.27 V for Au–BDNC–Au junctions; and 0.44 V, 0.58 V, 0.68 V, 0.76 V and 0.82 V for Au–BDA–Au junctions. Representative traces obtained in the experiments are shown in Supplementary Information section 6.3.

Estimating $Q_{\mathrm{P,Avg}}$ from the measured $\Delta T_{\mathrm{TC,Avg}}$. To relate the temperature rise of the thermocouple to the time-averaged power dissipation in the probe $Q_{\mathrm{P,Avg}}$, it is necessary to quantify the thermal resistance of the NTISTP. To elaborate, consider the resistance network shown in Fig. 1b, where the thermal resistances to heat flow in the probe (R_{P}), junction (R_{J}) and substrate (R_{S}) are identified. R_{P} was experimentally determined to be $72,800 \pm 500\,\mathrm{K\,W^{-1}}$ (see Supplementary Information). The thermal resistances of AMJs (R_{J}) are estimated to be at least $10^7\,\mathrm{K\,W^{-1}}$ for all the AMJs studied here (see Supplementary Information for more details). Thus, $R_{\mathrm{J}} \gg R_{\mathrm{P}}$ and therefore $\Delta T_{\mathrm{TC,Avg}}$ depends only on the power dissipated in the tip and is unaffected by the heating in the substrate. Thus, from a knowledge of $\Delta T_{\mathrm{TC,Avg}}$ and R_{P}, the time-averaged power dissipation, $Q_{\mathrm{P,Avg}}$, can be estimated as $Q_{\mathrm{P,Avg}} = \Delta T_{\mathrm{TC,Avg}}/R_{\mathrm{P}}$.

Computation of the transmission function. The zero-bias transmission functions shown in the manuscript were computed with the *ab initio* method described in detail elsewhere[24]. It is based on a combination of non-equilibrium Green's function techniques and density functional theory (DFT) and was implemented in the quantum-chemistry software package Turbomole. More details can be found in the Supplementary Information.

Computing the relationship between Q_{P} and Q_{Total}. We computed the power dissipated in the probe $Q_{\mathrm{P}}(V)$ and the total power dissipated in the junction Q_{Total} ($Q_{\mathrm{P}}(V) + Q_{\mathrm{S}}(V) = Q_{\mathrm{Total}}(V)$) using equation (1) and the zero-bias transmission curves of the molecular junctions (shown in Figs 2d and 3d). Subsequently, Q_{P} was plotted as a function of Q_{Total} as the relationship between Q_{P} and Q_{Total} is robustly predicted by our calculations (see Supplementary Information for details).